Plasma Sources Sci. Technol. **9** (2000) 183–190. Printed in the UK PII: S0963-0252(00)11531-2

Effect of different elementary processes on the breakdown in low-pressure helium gas

P Hartmann, Z Donkó, G Bánó, L Szalai and K Rózsa

Research Institute for Solid State Physics and Optics, PO Box 49, H-1525 Budapest, Hungary

Received 11 August 1999, in final form 26 January 2000

Abstract. We investigated the breakdown in low-pressure helium gas both experimentally and by computer simulations. At low breakdown voltages ($V_{BR} \leqslant 1000$ V) the experimental and simulation results show a good agreement (differences are within 20%), while at higher voltages the simulations and experiments agree qualitatively. Our simulations indicate that several processes contribute to the particular shape of the Paschen curve in helium at low pressures. These processes are: (1) the dependence of the (ion-induced) secondary electron emission yield on the ion energy, (2) the appearance of ion impact ionization of the gas at high electric fields and (3) the secondary electron emission from the cathode due to fast neutral atoms.

1. Introduction

The breakdown of gases—being one of the most fundamental phenomena in gas discharge physics—has been investigated since the beginning of gas discharge research and still attracts continuous interest [1–10]. Apart from the theoretical interest, the starting processes of the gas discharge have importance in a wide range of applications. The breakdown of the gas is also a crucial process in electric insulation, where it is to be avoided.

For plane–parallel electrode arrangements the Paschen law [11] states that the breakdown voltage is a function of the product of gas pressure (p) and electrode separation (d), $V_{BR} = f(pd)$. The Paschen curve usually exhibits a minimum corresponding to the lowest breakdown voltage. Both the $(pd)_{min}$ value where the minimum is found and the minimum breakdown voltage V_{BR}^{min} are characteristic for the gas and the cathode material.

The Paschen curve in helium gas has a particular shape in comparison with many other gases, see figure 1. Point 'A' indicates the Paschen minimum, while 'B' and 'C' correspond to the characteristic turning points of the curve. Penning found that at low pressures (below $pd \approx 2.2$ mbar cm) breakdown may occur at three different values of the voltage [1]. Besides helium, this type of behaviour was also observed in mercury vapour (see e.g. [4]). Although in previous work several attempts have been made to explain the shape of the Paschen curve in helium, it is still not completely understood [1, 2, 4, 7, 8, 11]. It is generally accepted that the energy dependence of the γ_i coefficient (electron emission yield for ion impact onto the cathode surface) and the ion impact ionization of buffer gas atoms ($He^+ + He \rightarrow He^+ + He^+ + e^-$) are responsible for the curve shape at low pressures [1, 4, 8, 11].

The aim of this work is to contribute to the understanding of the breakdown process in helium gas. We investigated the breakdown processes on the left (low pd) side of the Paschen curve. We developed a simulation program to describe the electron emission from the cathode and the motion of particles (electrons, He^+ ions and fast helium atoms) and their collisions in the discharge gap. An experiment was also carried out to verify the results of the calculations. The details of the experiment are described in section 2. The simulation model and the results are presented and discussed in section 3.1 and section 3.2. Section 4 summarizes the work.

2. Experiment

Our experimental discharge tube (see figure 2) had two flat disk copper electrodes with 36 mm diameter, facing each other at a distance of 10 mm. The electrodes were situated in a Pyrex tube of 40 mm inner diameter. The distance between the electrodes was maintained by an additional Pyrex ring which had, approximately, a 40 mm outer diameter and a 36 mm inner diameter. The base pressure of the (glass) vacuum system was in the order of 10^{-6} mbar and helium gas of 5.0 purity was used in the measurements. The discharge region was pumped through narrow (<0.1 mm) gaps between the Pyrex tube, spacer ring and the electrode disks. The pumping of the discharge volume was not very efficient through these gaps; however, after sufficient conditioning of the electrode surfaces (repetitive discharge and vacuum periods), reproducible data could be obtained in the experiments. The cleanliness of the system was checked by spectroscopic recording of the light emission spectrum from the discharge. Before the measurements of the

 © 2000 IOP Publishing Ltd

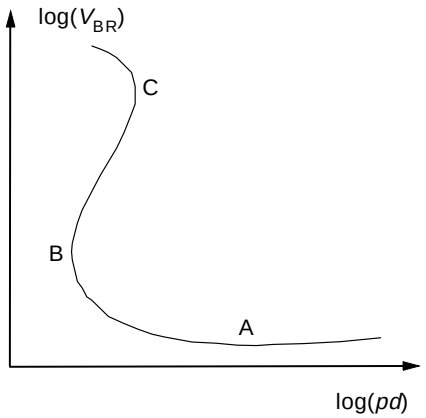

Figure 1. Schematic representation of the Paschen curve of helium. Point A indicates the Paschen minimum, while points B and C correspond to the characteristic turning points.

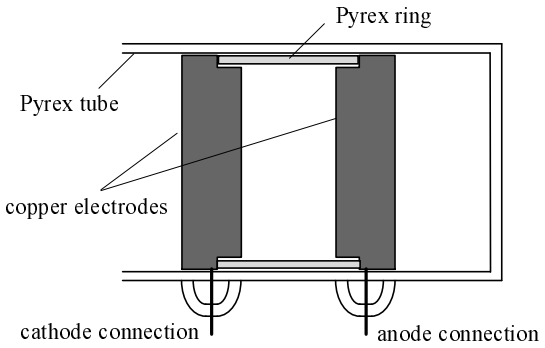

Figure 2. Schematic diagram of the experimental tube.

electrical characteristics (breakdown voltages), the surface of the cathode was conditioned by pulsed discharges (typically 1 ms pulses of 10–20 mA, at 3–5 mbar pressure for a total time of 15 min). This procedure resulted in acceptable reproducibility of breakdown voltages (∼10 V difference at the Paschen minimum from one day to another).

To determine the breakdown voltage (below voltages corresponding to point B shown in figure 1) we used the same method as used recently by Phelps and Jelenković [12]. The static voltage—current (V–I) characteristics of the discharge were measured for low current densities (between 0.01 and 0.2 μA cm^{-2}, where space charge effects can be neglected) and the voltage was extrapolated to zero current. The voltage obtained in this way is very close to the breakdown voltage [12]. To record the V–I curves, the discharge tube was connected through resistors ($R \approx 10$ MΩ) to a variable voltage source, and the discharge voltage and current were measured with digital multimeters. Figure 3(*a*) shows some of the results for different gas pressures. In the range of currents employed the characteristics show a slight positive slope which increases with decreasing pressure. It is noted that in most experiments—in agreement with theoretical expectations—a small negative slope is observed [10, 12, 13], but in some cases positive slopes also appear in the Townsend discharge regime [9, 14].

We note that the knowledge of the precise values of the circuit elements (resistors) is crucial for the correct evaluation

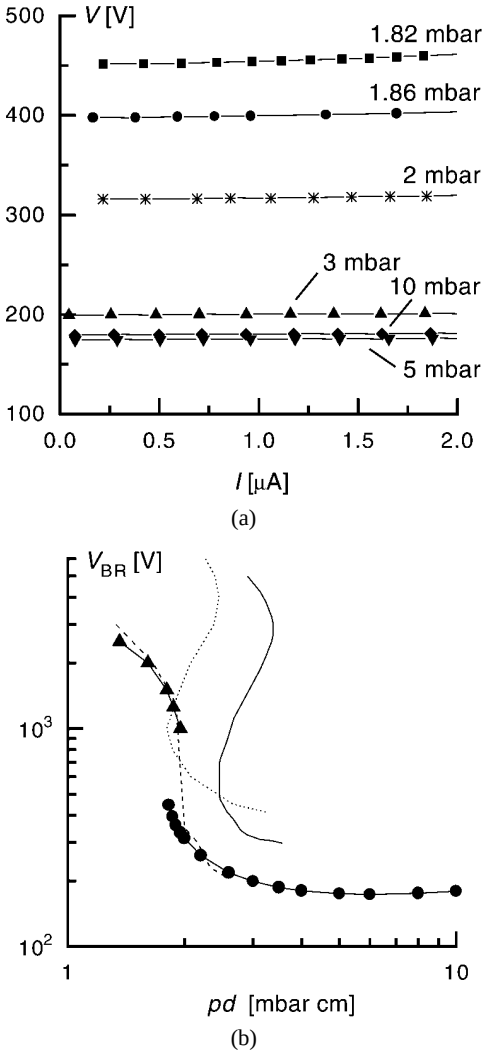

Figure 3. (*a*) Static electrical characteristics of the discharge for different pressures at low currents, (*b*) Paschen curves measured by different authors: (——) Penning [1], (- - - -) Jelenković and Phelps [10], (· · · · ·) Guseva [4] and our work: (——●——) static V–I curve measurements and (–▲–) 'gas-filling' method.

of the experimental data, as small errors of these values may induce large differences in the observed slope. To avoid this problem we have carefully calibrated the measurement using resistors of known values in the place of the discharge tube. Another phenomenon which can affect the measurement of electrical characteristics is the appearance of self-generated oscillations in the discharge [15, 16]. To exclude this effect we checked that no oscillations were present in the circuit in the current range used in the measurements. We suspect that the small positive slope of the V–I curves may originate from the effect of the somewhat distorted electric field distribution near the discharge tube wall, or from the presence of impurities in the discharge tube.

As the measurement of low-current, stationary V–I curves cannot be applied for the B–C section of the Paschen curve, we used a different (albeit probably less accurate) technique to determine the breakdown voltages higher than that corresponding to point B in figure 1. In this case the high voltage (up to 2.5 kV) was applied to the tube under vacuum.

Following this, the gas pressure was slowly increased, until breakdown of the gas occurred.

The measured Paschen curve is plotted in figure 3(*b*). The Paschen minimum occurs at $pd \approx 5.5$ mbar cm, and the minimum breakdown voltage was found to be ≈173 V in our experiments. The results of Penning [1], Guseva [4] and Jelenković and Phelps [10] are also plotted in the figure. The point B (see figure 1) corresponding to the minimum $(pd)_0$ for 'low-voltage breakdown' appears at ∼1.82 mbar cm for our case. Penning found 2.4 mbar cm, Guseva [4] and Jelenković and Phelps [10] give ∼1.75 and ∼2.0 mbar cm for $(pd)_0$, respectively. Our data are in very good agreement with recent experimental results of Jelenković and Phelps [10].

3. Simulation

3.1. Model

The motion of electrons, He^+ ions and fast He atoms in the electrode gap was traced by Monte Carlo simulation. The elementary processes considered in the model are listed in table 1 and their cross sections are plotted in figure 4(*a*). In the Monte Carlo simulation the equation of motion of the particles

$$q\boldsymbol{E}(x) = m\frac{\mathrm{d}^2\boldsymbol{r}}{\mathrm{d}t^2} \tag{1}$$

was integrated simultaneously with the equation assigning the length of the free flight

$$\int_{s_0}^{s_c} n\sigma[\varepsilon(s)]\,\mathrm{d}s = -\ln(1 - R_{01}) \tag{2}$$

where q, m, $\boldsymbol{r}$ and ε are the charge, mass, position and the kinetic energy of the particle, E is the electric field strength, n is the density of the gas, $\sigma(\varepsilon)$ is the sum of the energy-dependent cross sections of the collision processes of the traced particle, R_{01} is a random number uniformly distributed in the [0,1) interval, s is the curvilinear abscissa along the trajectory of the particle and s_0 and s_c denote the starting position of the free flight and the position of the next collision, respectively. The type of elementary process that occurred after a free flight was chosen randomly, taking into account the values of cross sections of the different collision processes at the given energy of the projectile. In the case of the electron and ion simulations we applied the null-collision technique to accelerate the speed of computation [17]. In the case of fast atoms (2) was solved directly for s_c as the energy of atoms does not change during the free flight.

The condition for the reproduction of charges in the discharge (which we also approximate as the condition for breakdown) is formulated as

$$\frac{1}{N}\left(\sum N_i(\varepsilon)\gamma_i(\varepsilon) + \sum N_f(\varepsilon)\gamma_f(\varepsilon)\right) = 1 \tag{3}$$

where $N_i(\varepsilon)$ and $N_f(\varepsilon)$ are the number of positive ions and fast atoms with energy ε arriving to the cathode due to the emission of N primary electrons. The γ_i and γ_f secondary electron emission coefficients depend on the energy of the impinging species. This condition ensures the reproduction of charges in electron avalanches (started by the emission of one primary electron from the cathode): the ions and fast atoms originating from an 'average' avalanche results in the emission of one 'new' primary electron.

The data for the secondary electron emission coefficients (given for a 'contaminated' copper surface) were taken from Hayden and Utterback [18], and are reproduced in figure 4(*b*). It is noted here that the secondary coefficients measured under ultrahigh vacuum conditions are usually not directly applicable to real discharges, as the presence of the gas and some other contaminants significantly alter the γ coefficients, see for example [19].

In the following, details of the processes listed in table 1 are presented.

3.1.1. Electron collisions with He atoms. The cross sections of electron collisions with He atoms (elastic scattering, electron impact excitation and ionization) were taken from [20, 21]. The elastic scattering was described by an anisotropic form of the $\sigma(\varepsilon, \chi)$ differential cross section [22–25]:

$$\frac{\sigma(\varepsilon, \chi)}{\sigma(\varepsilon)} = \frac{\varepsilon}{4\pi[1 + \varepsilon\sin^2(\chi/2)]\ln(1+\varepsilon)}. \tag{4}$$

The scattering angle χ was calculated by setting the cumulative distribution function of (4) equal to a random number uniformly distributed in the [0, 1) interval (see e.g. [24]):

$$\chi = \arccos\left(\frac{2 + \varepsilon\exp(R_{01}\ln(1+\varepsilon))}{\varepsilon}\right). \tag{5}$$

For the electron impact excitation process the specific energy levels of the atom are not considered, the energy loss of the electrons is randomly choosen between the first excitation level and the ionization level. When the electron energy is lower than the ionization potential, we assumed a random energy loss between the first excitation potential and the available electron energy. Formally

$$\Delta\varepsilon = -(\varepsilon_{exc1} + (\varepsilon^* - \varepsilon_{exc1})R_{01}) \tag{6}$$

where $\varepsilon^* = \min\{\varepsilon, E_i\}$, E_i is the ionization potential and ε_{exc1} is the energy of the first excited level. Due to the lack of data on differential scattering cross sections of electron impact excitation, we assumed that the scattering is isotropic.

In the ionization process the energy of the ejected (ε_1) and the scattered (ε_2) electrons is partitioned according to [26, 27]:

$$\varepsilon_1 = \omega\tan\left[R_{01}\arctan\left(\frac{\varepsilon - E_i}{2\omega}\right)\right] \tag{7}$$

$$\varepsilon_2 = \varepsilon - E_i - \varepsilon_1 \tag{8}$$

where ε is the energy of the electron before the collision and $\omega = 15$ in the case of helium gas [26–28]. The velocity vectors of the scattered and the ejected electrons are perpendicular to each other [17] and lie in the same plane with the velocity vector of the 'incoming' electron. The scattering angles χ_1 and χ_2 (measured with respect to the direction of

Table 1. Elementary processes considered in the model.

Process identification	Process	Name
1	$e^- + He \rightarrow e^- + He$	Elastic scattering
2	$e^- + He \rightarrow e^- + He^*$	Excitation
3	$e^- + He \rightarrow 2e^- + He^+$	Ionization
4	$He^+ + He \rightarrow He^+ + He$	Elastic scattering (including charge transfer)
5	$He^+ + He \rightarrow He_f + He^+$	Charge transfer
6	$He^+ + He \rightarrow He^+ + He^*$	2^1P excitation
7	$He^+ + He \rightarrow He^+ + He^+ + e^-$	Ionization
8	$He_f + He \rightarrow He_f + He_{(f)}$	Elastic scattering
9	$He_f + He \rightarrow He_f + He^*$	2^1P excitation
10	$He_f + He \rightarrow He_f + He^+ + e^-$	Ionization

Table 2. Parameters of cross sections fitted with the form $\sigma^{1/2} = A - B \ln \varepsilon$ for some collision processes. The energy ε is given in electron volts and σ is given in units 10^{-16} cm^2. The total elastic cross section includes the charge transfer cross section.

Process		A	B
$He^+ + He \rightarrow He^+ + He$	total elastic	7.04	0.620
$He^+ + He \rightarrow He^+ + He$	charge transfer	5.20	0.302
$He_f + He \rightarrow He_f + He_{(f)}$	elastic	4.79	0.492

velocity of the incoming electron) are calculated from (e.g. [17])

$$\cos \chi_1 = \left(\frac{\varepsilon_1}{\varepsilon - E_i} \right)^{1/2} \tag{9}$$

$$\cos \chi_2 = \left(\frac{\varepsilon_2}{\varepsilon - E_i} \right)^{1/2}. \tag{10}$$

The azimuth angle of the scattered electron is chosen randomly between zero and 2π for all collision processes.

3.1.2. Collisions of He^+ ions with He atoms. The processes included in our model are the elastic scattering of He^+ ions from He atoms and He^+ impact excitation and ionization of He atoms. The elastic scattering contains the symmetric charge transfer process as a special case (elastic backscattering). In figure 4(*a*) the total elastic and the charge transfer collision cross sections are plotted. These cross sections were taken from Cramer and Simons [29], and the data were fitted to a functional form

$$\sigma^{1/2}(\varepsilon) = A - B \ln \varepsilon. \tag{11}$$

The parameters A and B for these processes are given in table 2.

The only He^+ impact excitation process considered is that of the 2^1P level. This process has a threshold energy of ≈60 eV (lab frame) and a cross section in order of 10^{-17} cm^2 at 100 eV He^+ energy [30]. The cross sections for the excitation of other levels by He^+ ions are at least an order of magnitude lower [31].

The ionization cross section of He atoms by He^+ ions is in the same order of magnitude as the 2^1P excitation at ion energies of few hundred eV [32]. Thus this process may be an important source of ionization at high voltages.

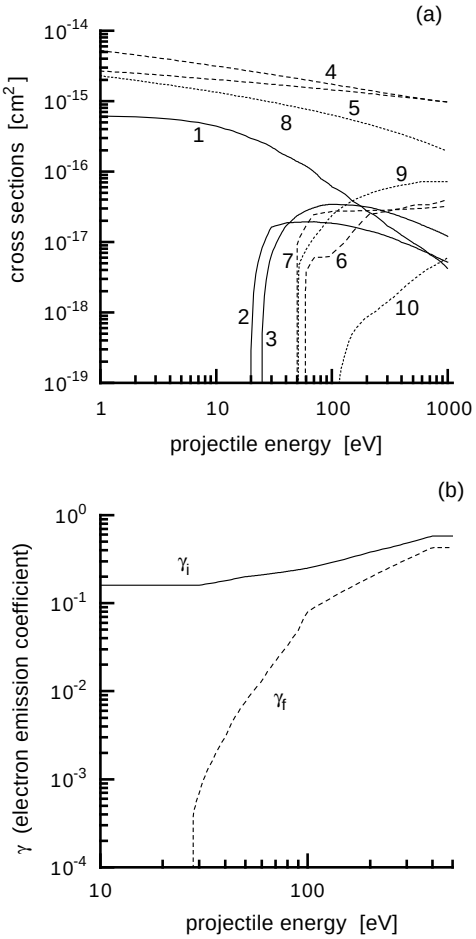

Figure 4. (*a*) Cross sections and (*b*) γ coefficients against projectile energy. (*a*) 1, elastic scattering of electrons; (2), electron-impact excitation; (3), electron-impact ionization; (4), total elastic scattering of ions; (5), ion–atom symmetric charge transfer; (6), ion-impact excitation; (7), ion-impact ionization; (8), elastic scattering of atoms; (9), atom-impact excitation; and (10), atom-impact ionization. (*b*) γ_i, ion impact; and γ_f, fast atom impact.

In the case of elastic collision, ion impact excitation and ionization, the scattering was assumed to be isotropic in the centre-of-mass system. In the charge exchange process the ion was assumed to start with thermal energy and the fast atom resulting from the process started with the velocity of the colliding ion.

3.1.3. Collisions of fast He atoms with He gas. In the case of fast He atoms we considered elastic collisions from He atoms and the excitation and ionization of He atoms. The elastic scattering cross section was taken from Jordan and Amdur [33] who presented measurements between 100 and 400 eV. Their data were fitted and extrapolated towards lower energies with a form given by (11). This extrapolation resulted a cross section at thermal energies which was in good agreement with thermal energy data [34–38].

The excitation cross section of the 2^1P level was taken from [39]; the data in this paper indicate that the excitation to higher lying levels of He occurs with significantly lower cross sections. The ionization cross section of He by fast He atoms was taken from the experimental data of Hayden and Utterback [18]. This process becomes important above 100 eV energy and has an order of magnitude lower cross section than ionization by He^+. Because of the lack of reliable differential cross sections, all collision processes involving fast atoms were assumed to be isotropic in the centre-of-mass system.

3.1.4. Surface processes. The primary electrons were started from the cathode with an initial kinetic energy between 0 and 10 eV. Some of the electrons emitted from the cathode can be backscattered to the cathode after taking part in the first elastic collision process. These low-energy electrons can be absorbed by the cathode or reflected from the cathode and they can also induce the emission of a 'new' electron. The data for these processes were taken from [40, 41].

In our simulations we also considered the backscattering of fast electrons from the anode of the discharge. These electrons—especially at low pressures—have a significant influence on the ion production rate in the electrode gap, thus affecting the breakdown voltage. The probability of electron backscattering from the copper anode surface was taken to be $\eta_0 = 0.36$, from [42]. The dependence of η on the angle of incidence α was approximated as:

$$\eta(\alpha) = 0.36 \exp\{B(1 - \cos\alpha)\} \qquad (12)$$

where $B = 0.92$ was used in accordance with the data given in (for electrons of 1 keV energy) [42]. The energy distribution of electrons backscattered from the anode was approximated based on the data given in [43].

3.2. Results and discussion

In figure 5(*a*) the low-voltage part of our calculated curve is plotted and compared with our experimental data; good agreement (∼20% difference) between these two data sets is found. The Paschen curve calculated from our model is plotted up to $V_{BR} \approx 10^4$ V in figure 5(*b*) in comparison with previous and present experimental data (shown in figure 3(*b*)). The results of the simulations and our experimental data agree only qualitatively on the left-hand side of the Paschen curve. Using the same data, the reduced electric field E/n at breakdown is plotted as a function of nd in figure 5(*c*). In this representation the characteristic parts of the Paschen curve can also be identified.

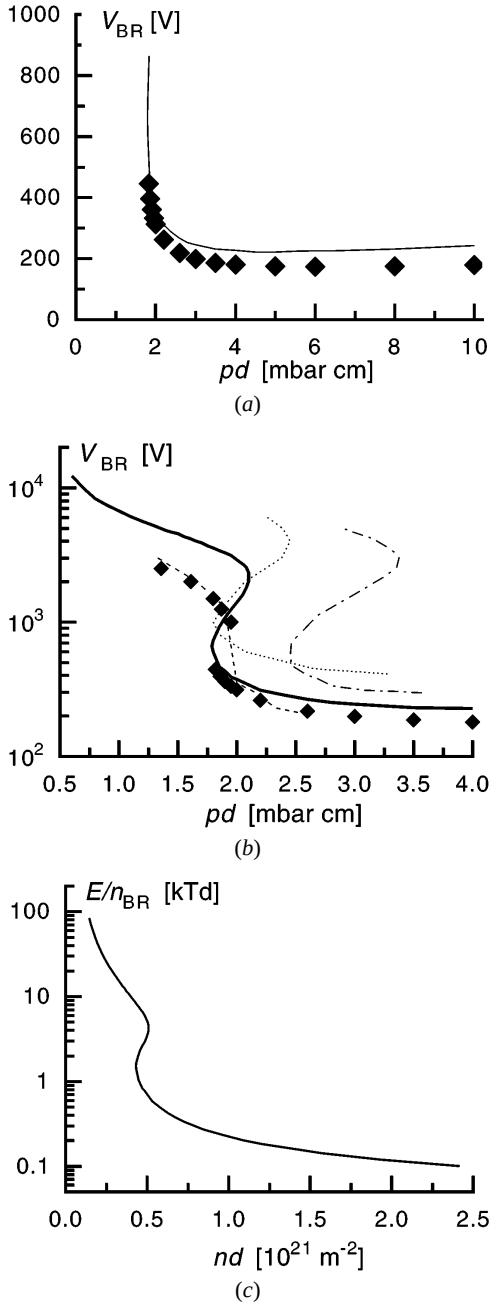

Figure 5. Simulated Paschen curves: (*a*) comparison of the calculated (——) and our measured (♦) Paschen curves and (*b*) the result of our simulation (——) in comparison with: (— · —) Penning [1], (– – –) Jelenković and Phelps [10], (· · · · · ·) Guseva [4] and our experimental results (♦). (*c*) Reduced electric field E/n at breakdown as a function of nd.

The particular shape of the Paschen curve can be understood by analysing the processes responsible for the charge reproduction. In figure 6(*a*) the contributions of the different (electron, ion and fast atom impact) ionizing processes to the total ion production are displayed. Figure 6(*b*) shows the contributions of the positive ions and the neutral atoms to the emission of primary electrons from the cathode. Both these data sets are given as a function of the reduced electric field E/n, as they are not unique functions of the gas pressure. The results of the simulations show that on

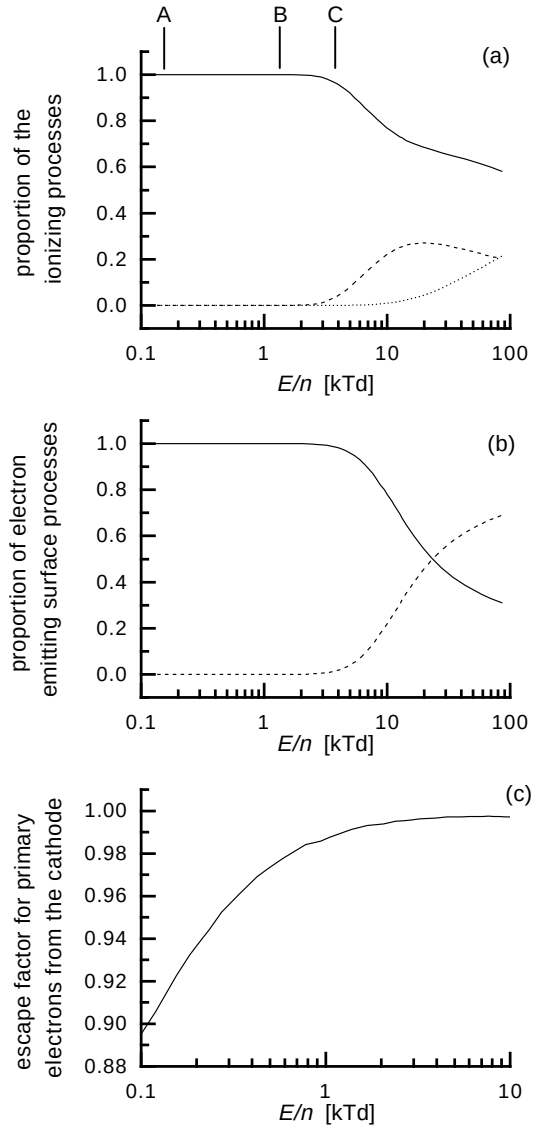

Figure 6. (*a*) Proportion of ionizing processes: (——) electron-impact ionization, (- - - -) ion-impact ionization, (· · · · · ·) atom-impact ionization. (*b*) Proportion of primary-electron emitting surface processes: (——) ion-impact electron emission, (– – –) neutral-atom-impact electron emission (A, B and C indicate the points shown in figure 1.). (*c*) The escape factor for primary electrons.

the A–B section of the Paschen curve (and at higher pressures from point A, see figure 1) the only important processes in the self-maintenance of the discharge are the electron impact ionization and the electron emission from the cathode due to He^+ impact. (The Paschen minimum $(pd)_{min}$ found experimentally corresponds to $E/n = 0.13$ kTd, where 1 kTd $= 10^{-18}$ Vm^2.) On the B–C section of the curve still the electron impact ionization dominates in the production of ions. The E/n values corresponding to points B and C are 1.5 and 4.3 kTd, respectively. The number of ions produced by a primary electron decreases with increasing voltage, but the increase of γ_i with the kinetic energy of the ions compensates for this. With further increasing voltage—above point C—electron emission from cathode due to fast He atoms plays an important role, as it can be seen in figure 6(*b*). This process already accounts for approximately 20% of primary electron production at $V = 4000$ V ($E/n = 10$ kTd). At these conditions positive ion impact causes approximately 25% of the ionization while fast He atoms have only a share of 1%.

On the 'right-hand side' of the Paschen curve (at pressures higher than that corresponding to the Paschen minimum $(pd)_{min}$, point A in figure 1) the breakdown voltage slowly increases with increasing pressure. This increase is attributed to the fact that with increasing pressure gradually more electron energy is deposited into excitation. Apart from this effect, another phenomenon also influences the breakdown voltage at higher pressures. While at high values of E/n, almost all of the primary electrons leave the vicinity of the cathode, at low E/n some of the primary electrons may be backscattered and absorbed by the cathode. Our simulations also made it possible to determine the so-called escape factor [19, 44], which is defined as the probability of that a primary electron leaves the vicinity of the cathode after being emitted from the cathode. The escape factor decreases with decreasing E/n and this also contributes to the increasing breakdown voltage. Figure 6(*c*) shows the escape factor as a function of E/n. The data indicate that around the Paschen minimum the escape factor is approximately 0.92 and decreases to 0.9 at a pressure of 10 mbar ($E/n = 0.1$ kTd).

To investigate the effect of certain elementary processes on the shape of the Paschen curve, we also carried out simulations in which we ignored some of the processes. Together with the results of the simulations including all the elementary processes listed in table 1, figure 7(*a*) shows the Paschen curves obtained by neglecting:

(i) processes initiated by fast neutral atoms,
(ii) ionization by ion impact,
(iii) both of the above processes.

The results show that below about 1000 V the processes ignored have no effect on the breakdown voltage. At higher voltages, however, both the fast-atom-initiated processes and He^+ impact ionization have a significant effect on the breakdown voltage. All these observations are in agreement with earlier explanations of the shape of the Paschen curve in helium, except that we also identify the electron emission due to fast neutral bombardment of the cathode as an important process.

The simulations were also carried out with different assumptions for the backscattering of electrons from the anode. Figure 7(*b*) illustrates the dependence of the breakdown voltage on the backscattering probability of electrons from the anode. Together with the breakdown voltage data obtained using the assumptions given in section 3.1.4 we also displayed the Paschen curves with two different assumptions:

- no backscattering ($\eta = 0$),
- using $\eta = 0.25$, based on the data of Sternglass [45].

While the highest backscattering probability results in $(pd)_{min} \approx 1.75$ mbar cm for low-voltage breakdown, $\eta = 0$ shifts this value above 2 mbar cm. These data emphasize that besides the material and surface conditions of the cathode, the properties of the anode can also significantly

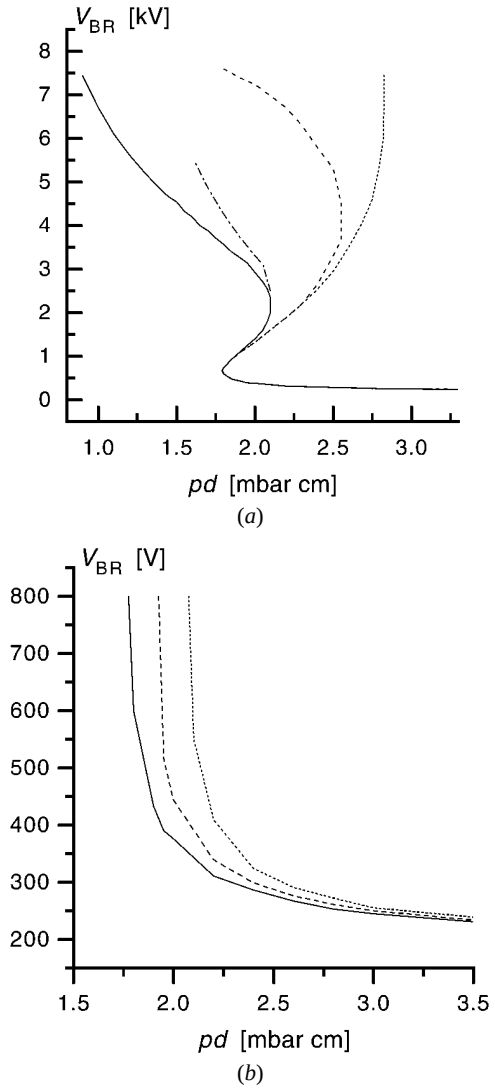

Figure 7. (*a*) Importance of different elementary processes: (——) full simulation, (— · —) ignoring fast atoms, (- - - -) ignoring ion-impact ionization, (· · · · · ·) ignoring fast atoms and ion-impact ionization; (*b*) Effect of electron backscattering from the anode: (——) $\eta = 0.36 \exp(0.92(1 - \cos\alpha))$, (- - - -) $\eta = 0.25$ and (· · · · · ·) $\eta = 0$.

influence the breakdown voltage at low pressures. In order to minimize the effect of electron backscattering from the anode, materials with low backscattering probability (e.g. graphite) are frequently used in discharge experiments [12, 46–48].

4. Summary

We investigated the breakdown of helium gas at gas pressure $\times$ electrode separation below 10 mbar cm experimentally and by a simulation model. In the experiment the breakdown voltage was determined by extrapolating the voltage of the low-current ($j \leqslant 0.2\ \mu$A cm^{-2}) dc discharge to zero current. This method allowed us to measure the breakdown voltage on the 'low-voltage' branch of the Paschen curve. Using a different technique—slowly increasing the gas pressure while the voltage was already applied to the tube—we could also determine the breakdown voltage on the 'high-voltage' branch of the Paschen curve.

The simulation of the motion of electrons, helium ions and fast helium atoms made it possible to calculate the Paschen curve for helium. On the 'low-voltage' branch of the Paschen curve we obtained a good agreement (≈20% difference) between the experimental data and the simulation results. The data points obtained by the gas-filling method agree very well with previously published data of Jelenković and Phelps [10], and are in a good qualitative agreement with our present simulation results.

Our simulation results indicate that the particular shape of the Paschen curve is due to three important processes:

(i) dependence on the He^+ energy of the electron emission yield from the cathode,
(ii) the appearance of He^+ production at high electric fields in He^+–He collisions,
(iii) electron emission from the cathode due to the impact of fast He atoms originating from symmetric charge transfer process.

The first two of these processes have already been identified in earlier studies as important processes influencing the charge production at low pressures [1, 2, 4, 7]. The present results show that fast-atom-induced electron emission from the cathode is also an important process.

We have also demonstrated the effect of individual collision processes on the Paschen curve as well as the effect of electron backscattering from the anode.

Acknowledgments

The authors thank Professor A V Phelps for useful discussions. This work was supported by the Hungarian Science Foundation through the grant OTKA-T-25989, OTKA-T-25941 and OTKA-F-25503. The construction of the discharge tube by T J Forgács, J Tóth, E Sárközi and Gy Császár is gratefully acknowledged.

References

[1] Penning F M 1931 *Proc. R. Acad. Amst.* **34** 1305
[2] Meek J M and Craggs J D 1953 *Electrical Breakdown of Gases* (Oxford: Clarendon)
[3] Ward A L and Jones E 1961 *Phys. Rev.* **122** 376
[4] Guseva L G 1964 On discharge striking in polyatomic gases at $(pd) < (pd)_{min}$ *Investigations into Electrical Discharges in Gases* ed B N Klyarfeld (New York: Macmillan)
[5] Bortnik I M 1968 *Sov. Phys. Tech. Phys.* **13** 769
[6] Schönhuber M J 1969 *IEEE Trans. Power Apparatus Syst.* **88** 100
[7] Parker A B and Johnson P C 1971 *Proc. R. Soc.* A **325** 511
[8] Hillmann H, Müller F and Wenz H 1994 *Plasma Sources Sci. Technol.* **3** 496
[9] Auday G, Guillot Ph, Galy G and Brunet H 1998 *J. Appl. Phys.* **83** 5917
[10] Jelenković B M and Phelps A V 1998 *Bull. Am. Phys. Soc.* **43** 5 1432
[11] Francis G 1956 The glow discharge at low pressure *Encyclopedia of Physics* ed S Flügge (Berlin: Springer)
[12] Phelps A V and Jelenković B M 1988 *Phys. Rev.* A **38** 2975

[13] Stefanović I and Petrović Z Lj 1997 *Japan. J. Appl. Phys.* **36** 4728
[14] Rao M V V S, Van Brunt R J and Olthoff J K 1996 *Phys. Rev.* E **54** 5641
[15] Petrović Z Lj, Stefanović I, Vrhovac S and Živković J 1997 *J. Physique IV* **7** C4-341
[16] Petrović Z Lj and Phelps A V 1993 *Phys. Rev.* E **47** 2806
[17] Boeuf J P and Marode E 1982 *J. Phys. D: Appl. Phys.* **15** 2169
[18] Hayden H C and Utterback N G 1964 *Phys. Rev.* **135** A1575
[19] Phelps A V and Petrović Z Lj 1999 *Plasma Sources Sci. Technol.* **8** R21
[20] Nickel J C, Imre K, Register D F and Trajmar S 1985 *J. Phys. B: At. Mol. Phys.* **18** 125
[21] de Heer F J and Jansen R H J 1977 *J. Phys. B: At. Mol. Phys.* **10** 3741
[22] Bogaerts A 1996 Mathematical modeling of a direct current glow discharge in argon *PhD Thesis* University of Antwerp
[23] Surendra M, Graves D B and Jellum G M 1990 *Phys. Rev.* A **41** 1112
[24] Birdsall C 1991 *IEEE Trans. Plasma Sci* **19** 65
[25] Lymberopoulos D P and Schieber J D 1994 *Phys. Rev.* E **50** 4911
[26] Yoshida S, Phelps A V and Pitchford L C 1983 *Phys. Rev.* A **27** 2858
[27] Opal C B, Peterson W K and Beaty E C 1971 *J. Chem. Phys.* **55** 4100
[28] Ouadoudi N 1994 Simulation numérique de la phase d'initiation d'une décharge à cathode creuse de type pseudospark *PhD Thesis* Université Paul Sabatier, Toulouse
[29] Cramer W H and Simons J H 1985 *J. Chem. Phys.* **26** 1272
[30] Okasaka R, Konishi Y, Sato Y and Fukuda K 1987 *J. Phys. B: At. Mol. Phys.* **20** 3771
[31] Barnett C F 1990 *Atomic Data for Fusion: Collision of H, H_2, He and Li Atoms and Molecules* ed H T Hunter *et al* (Oak Ridge National Laboratory Report ORNL-6086/V1)
[32] Gilbody H B and Hasted J B 1957 *Proc. R. Soc.* A **240** 382
[33] Jordan J E and Amdur I 1967 *J. Chem. Phys.* **46** 165
[34] Massey H S W, Burhop E H S and Gilbody H B 1971 *Electronic and Ionic Impact Phenomena: Slow Collisions of Heavy Particles* vol 3 (Oxford: Calderon) p 1411
[35] Beier H J 1966 *Z. Phys.* **196** 185
[36] Rothe E W and Neynaber R H 1965 *J. Chem. Phys.* **43** 4177
[37] Harrison H 1962 *J. Chem. Phys.* **37** 1164
[38] Moore G E, Datz S and van der Valk F 1967 *J. Chem. Phys.* **46** 2012
[39] Kempter V, Veith F and Zehnle L 1975 *J. Phys. B: At. Mol. Phys.* **8** 1041
[40] Myers H P 1952 *Proc. R. Soc.* A **215** 329
[41] Harrower G A 1956 *Phys. Rev.* **104** 52
[42] Darlington E H and Cosslett V E 1972 *J. Phys. D: Appl. Phys.* **5** 1969
[43] Jardin C, Kessas S, Khelifa B, Bondott P and Gruzza B 1991 *J. Phys. D: Appl. Phys.* **24** 1115
[44] Nagorny V P and Drallos P J 1997 *Plasma Sources Sci. Technol.* **6** 212–19
[45] Sternglass E J 1954 *Phys. Rev.* **95** 345
[46] Jelenković B M and Phelps A V 1987 *Phys. Rev.* A **36** 5310
[47] Stojanović V D, Jelenković B M and Petrović Z Lj 1997 *J. Appl. Phys.* **81** 3 1601
[48] Stojanović V D and Petrović Z Lj 1991 *J. Phys. D: Appl. Phys.* **31** 834